A. Binder[1]

W. Forster

K. Mach

H. Rogge

Research Engineers,
DFVLR—Propulsion Institute,
Cologne, Federal Republic of Germany

Unsteady Flow Interaction Caused by Stator Secondary Vortices in a Turbine Rotor

Nonintrusive measurements near and within the rotor of a cold-air turbine showed a sudden increase of turbulence energy when the wake portion of the incoming fluid entered the rotor. It has been suggested that this was due to the cutting of the passage vortices and trailing-edge shed vortices which emerge from the stator row. Since these secondary vortices are located very close to the stator wakes, it was very difficult to distinguish between the effects of shed vortex and passage vortex cutting on turbulence intensification. In the present paper, a method is shown which, with the help of time-distance diagrams, made it possible to attribute the turbulence increase to the breakdown of the secondary vortices. Further, the time-distance diagrams made it possible to locate the origin of turbulence production and follow the spreading of the highly turbulent flow regions through the rotor channel.

Introduction

An observer moving with a turbine rotor sees the incoming flow as a sequence of regions of high-velocity and small random velocity fluctuations, i.e., free-stream flow, alternating with regions of lower velocity, high turbulence, and a number of vortices, i.e., wake flow. Both kinds of flow enter the rotor obliquely, striking the pressure side channel before the suction side. Each time a wake region strikes the pressure side, the observer sees an area of increased turbulence, higher than in the incoming wake flow, form on the pressure-side nose and spread across the channel as it is swept downstream.

An observer standing outside the turbine and looking in sees the flow field as depicted in Fig. 1 for one instant in time [5, 9]. The stator wake and secondary vortices leave the stator with absolute angle α with reference to the circumferential direction. Because of the rotor motion, they enter it with relative angle β, striking the pressure-side blade first. As will be shown, the region of increased turbulence propagates back down the wake, which assumes a bowed shape because the velocity in midchannel is higher than in the stagnation region [6, 12]. The roles played by the wake and secondary vortices are difficult to separate because they lie parallel and close to, sometimes even coincident with, one another [2]. However, since it has been shown that unsteady phenomena significantly affect turbomachinery flow and performance, any contribution to their understanding offers the possibility of improved performance in future designs. A recent test series at the DFVLR in Cologne consisted of a careful mapping of the nonstationary and time-averaged flow fields in a turbine rotor; several papers have described different aspects of the work [2–6]. In this paper we propose a mechanism relating the spread of augmented turbulence across the blade channel to the collapse of the stator secondary vortices and describe how the vortices can be identified against the background of the wake flow.

Experimental Apparatus

The research turbine consisted of a single, uncooled, weakly transonic stage, whose essential features are shown schematically in Fig. 2. The stator had 20 airfoils and the rotor had 31. Because of the low aspect ratios (stator 0.56, rotor 0.9) the flow was fully three dimensional and, because the axial

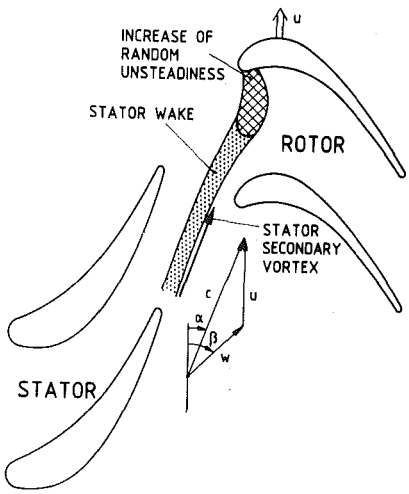

Fig. 1 Schematic of wake and vortex interaction process

[1] Presently at Motoren- und Turbinen-Union, Munich.

Contributed by the Gas Turbine Division of THE AMERICAN SOCIETY OF MECHANICAL ENGINEERS and presented at the 31st International Gas Turbine Conference and Exhibit, Düsseldorf, Federal Republic of Germany, June 8–12, 1986. Manuscript received at ASME Headquarters February 28, 1986. Paper No. 86-GT-302.

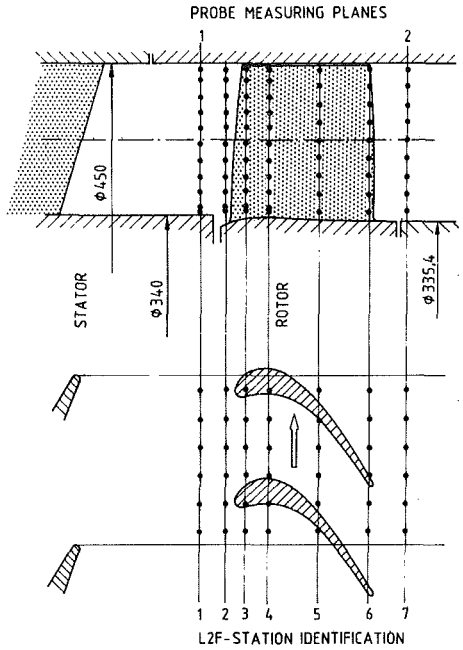

Fig. 2 L2F locations

distance between rotor and stator had been made relatively large in order to provide room for stator exit survey probes, potential (or inviscid) interactions between blade rows could be neglected as a source of nonstationary effects, leaving only the alternating impact of free stream and wake plus secondary vortices as sources of instationary flows into the rotor. Further details of the construction of the rig can be found in [2, 3]. For this test series, a part-load operating point was chosen which, for an average stator exit Mach number of 0.82 and rotor speed of 7800 rpm, yielded approximately zero incidence and completely subsonic flow through the rotor [2]. At each of the points marked with a heavy dot in Fig. 2, a laser-two-focus (L2F) velocimeter measured the ensemble-averaged flow velocity and direction and the components of the random fluctuating velocity parallel and perpendicular to the flow direction. The phenomena described in this paper – the wake and secondary vortex cutting and subsequent vortex breakdown accompanied by the appearance of a region of augmented turbulence – occur before the flow passes through L2F plane 4.

The operating principle of the L2F velocimeter will be only briefly reviewed here. For further details, see [14, 15]. At the desired measurement point, e.g., one of those in the $11 \times 6 \times 7$ array shown in Fig. 2, two laser beams are focused and aligned so that two spots of light form about 0.3 mm apart in the flow direction. As tiny particles (in this case, 0.1-μm oil droplets) are carried through the two spots by the gas stream, the light reflected from them is detected and used to compute the travel time between the two spots. Similarly, two components of the turbulent fluctuating velocity can be measured. A sufficiently large number of data are collected at each point for each of 16 rotor angular positions to allow calculation of statistical averages (phase-locked averaging) [5].

Data Analysis via Time-Distance Diagrams

The flow quantities velocity, direction, etc., in the unsteady three-dimensional flow field of a turbomachine depend on four variables (axial, radial, and circumferential position and time). However, it is not possible to describe this four-dimensional dependence in a straightforward manner. Usually at least two independent variables have to be held constant or averaged. In the initial analyses of the laser anemometry data, the time and either radial or axial coordinate were selected. This yielded a circumferential or axial view of a momentary or time-averaged flow situation. In this investigation, the axial and radial coordinates were held constant and the temporal variation of the flow quantities in the circumferential direction was analyzed by means of time–distance diagrams [3].

Figure 3 shows a schematic example for an axial position ahead of the rotor at midspan. The boundaries in the circumferential direction are on lines which touch the leading edges of two adjacent rotor blades with the design relative inlet angle β (upper figure). An observer moving with the rotor, i.e., in the relative frame of reference, notices an unsteady flow which is periodic with the stator pitch. At each circumferential position between the pressure side (*PS*) and suction side (*SS*) boundary, a perturbation of the incoming flow in the absolute frame (e.g., the wake) is felt at a different time; at the time t no part of the rotor entrance region is influenced by the stator wake. As the rotor moves on, the (stator) suction side of the wake is first felt at the pressure-side boundary of the rotor *PS*. As the rotor continues to move, the rest of the wake passes through *PS*. Locations which are closer to the suction-side end *SS* of the line notice the wake later.

This passage of the wake through the line *PS–SS* appears in the time–distance diagram (Fig. 3, lower) as an oblique line. With proper choice of scale, disturbances which travel along the line with rotor speed are inclined to the horizontal direction with an angle $\theta = 45$ deg. Smaller angles indicate a lower velocity of the disturbance in the circumferential direction and vice versa.

Due to the rotor potential field, a fluid filament which was straight in the absolute frame leaving the stator region (e.g., a filament of the wake) is distorted when it passes through the rotor channel. The deformation of the fluid filament was traced through the measured unsteady flow field with the assumption of two-dimensional flow [6]. In Fig. 4 (left side) a filament is shown entering the upper left corner of the measurement area with absolute inflow angle α_1. The succeeding lines show the filament being convected through the rotor by the nonstationary relative flow. The time interval between two lines is 1/6 of the stator pitch. Near the stagnation pressure fields at the leading edges, the flow is decelerated and the fluid filament becomes bowed.

In the time–distance diagram the deformation of the fluid filament appears as shown in Fig. 4 (right). For axial position I the influence of the rotor potential flow field is weak. The par-

Nomenclature

c = absolute velocity
c' = absolute velocity fluctuation (random part)
L2F = laser-two-focus
PS = pressure side
r = radius
SS = suction side
t = time
T = time period
u = rotational velocity
w = relative velocity
x, y = coordinates
α = absolute flow angle (yaw)
β = relative flow angle (yaw)
θ = slope

Subscripts and Superscripts

1, 2, . . . ,6 = location
L = parallel to absolute velocity
$\tilde{}$ = ensemble averaged
$\hat{}$ = time averaged

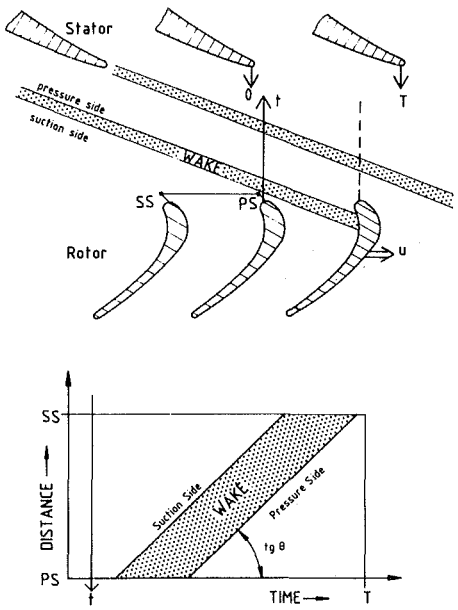

Fig. 3 Relationship between time-distance diagram and physical space

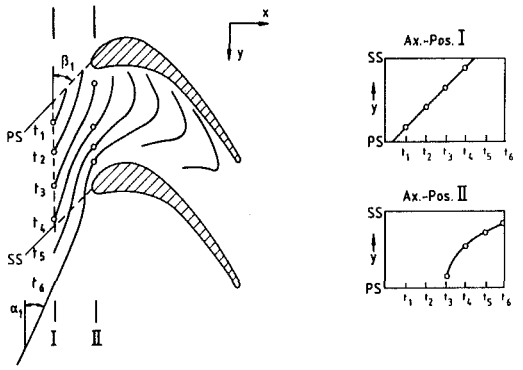

Fig. 4 Filament deformation in the rotor

ticles of the filament cross the circumferential line with their original axial velocity c_x and the intersection of the filament and the line moves from pressure side to suction side with rotor speed; therefore, the filament appears as a straight line with a 45 deg slope. At axial position II the deformation of the filament distorts this trajectory. Near the pressure side of the rotor the inclination is higher, which means that this end of the filament passes more nearly broadside through the line. As the suction side of the adjacent rotor blade gets closer to the filament, the circumferential velocity of the filament is reduced and the inclination of its trajectory in the time-distance diagram becomes smaller.

Locating the Vortex Centers

Behind the stator, the secondary vortices are located in the wake or in its immediate vicinity [2, 4] and it is therefore difficult to track their positions or to relate an observed phenomenon to one or the other. Especially in the rotor region, where the wake and the vortices are cut up by the blades, this fact causes significant difficulties in analyzing the measured results.

In order to get a better understanding of the flow phenomena associated with stator secondary flows, the vortex centers, or axes, were traced as fluid filaments. Behind the stator and in front of the rotor entrance region, these axes are aligned in the absolute flow direction [8, 11]. The original shape and the subsequent deformation of the filaments as they pass through the rotor are shown in Fig. 4. The initial positions of the filaments, which are necessary to calculate the convective deformation, were determined from the distributions of random unsteadiness and yaw angle in L2F plane 1 (Fig. 6).

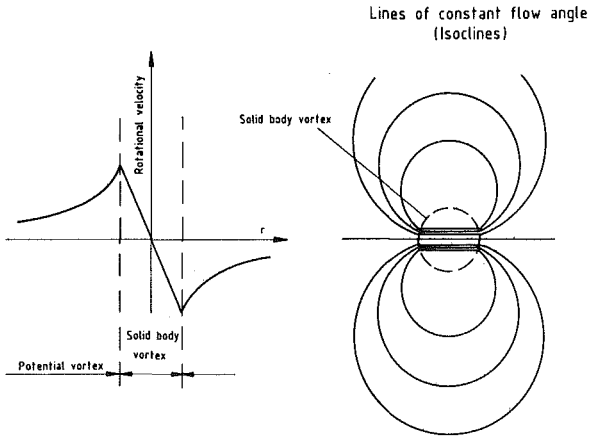

Fig. 5 Isoclines of a real (Rankine) vortex

As described in [4], secondary vortices can be located by means of yaw angle contours. In such yaw angle distributions, the rotation of a secondary vortex leads to characteristic shapes of the isoclinal lines (Fig. 5). A solid body rotation, which is located in the center of every real vortex, is characterized by straight parallel isoclines, usually aligned in the circumferential direction [3]. A free vortex, which usually forms the outer part of a real vortex, is characterized by two groups of circles tangent at the vortex center. Which of these groups indicates underturning or overturning depends on the sense of rotation. This simple model [4] was developed for a measuring plane perpendicular to the vortex axis. In the case of measurement plane 1 (Fig. 2), the secondary vortex axis and the absolute flow direction are inclined about 22 deg to the measurement plane. Consequently, the circles indicating a free vortex flow appear as ellipses whose major axes are about three times longer than their minor axes. By means of this simple model, vortices can be identified in an isoclinal contour map.

Discussion of Results

Four vortices can be found in plane 1 by applying the model just described. In the lower part of Fig. 6, vortices I and II are the well-known passage vortices which arise within the stator passage. Passage vortex I rotates in the clockwise direction, causing overturning and therefore lower values of the flow angle near the casing, and underturning (higher values of $\hat{\alpha}$) on the opposite side of the vortex center. Passage vortex II, which rotates in the opposite direction, is much smaller than passage vortex I because of the radially inward movement of the flow behind the stator [4], causing passage vortex II to move away from the casing and toward the hub. Therefore, vortex I rotates largely free from wall effects, whereas vortex II is suppressed by the hub. Two other vortices, associated with trailing shed vorticity or the remainder of the suction-side leg of the horseshoe vortex, exist in the midspan area.

As seen in the lower part of Fig. 6, the low aspect ratio of the stator leads to secondary vortices, for example III and IV, which are distributed along the entire vane height.

The four vortices whose centers are marked by dashed circles are also marked in the random unsteadiness distribution of the same plane (upper part of Fig. 6). In this figure, the dark contour line indicates the approximate boundary between high and low-turbulence flow regions. The low-turbulence flow indicates the core flow, which is essentially free from viscous effects. The regions showing high turbulence are the wakes and the secondary "loss cores" at the suction

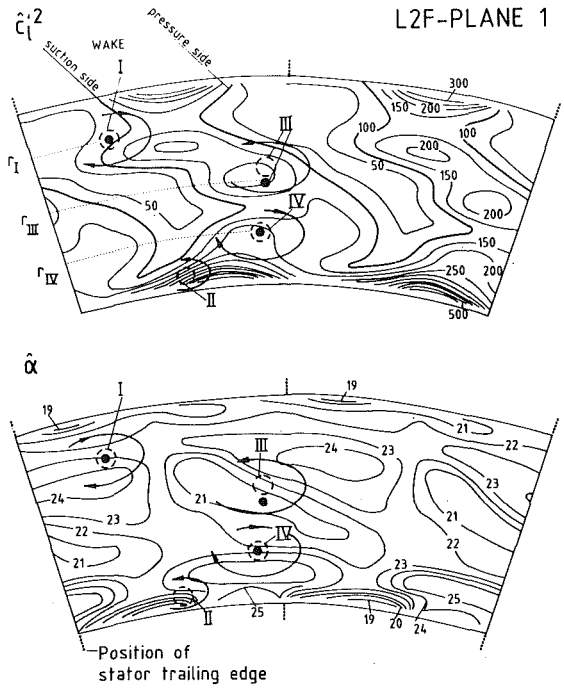

Fig. 6 Contours of time-averaged random unsteadiness $\hat{c}_L'^2$ and absolute flow angle $\hat{\alpha}$ in L2F plane 1

sides of the wakes. These secondary "loss cores" [4], which are located near the hub and the shroud, arise inside the stator passages due to boundary layer accumulation. The accumulation on the suction side of the vanes is caused by the rotational motion of the passage vortices and the cross-passage pressure gradient. Downstream of the stator, i.e., in the wake, these high-loss, high-random-unsteadiness regions [5] are located in or near the centers of the passage vortices.

Looking at the location of the vortex centers relative to the wake, it is apparent that the passage vortices I and II are located at the suction side of the wake, while the secondary vortices III and IV are located within the wake. The location of vortex center III is between the middle of the wake and the pressure side and secondary vortex IV is shifted toward the suction side. The origins of the fluid filaments with which the convection of the stator secondary vortices were followed through the rotor are marked by black dots. Two filaments were located at radii r_I and r_{IV}, corresponding to the centers of vortices I and IV. The filament indicating vortex III is shifted slightly outside the vortex center because no radial measurement location was available at the center itself (Fig. 2).

In the following diagrams the locations of the filaments leaving these dots are always marked by a thick black line.

Figure 7 shows the time history of vortex I from Fig. 6 as it passes through the four axial measurement planes in the rotor entrance region. In the first picture, the vortex and wake pass through L2F plane 1, approximately 25 percent of axial chord upstream of the nose. The vortex center lies toward the suction side of the wake. Recalling from Fig. 1 that the vortex and wake leave the stator with absolute angle α but enter the rotor with relative angle β, we see their intersection with the plane sweep from pressure side to suction side as time advances, i.e., as they pass through the plane (see also Fig. 3). The straight path of the vortex center means that all parts of the vortex pass through the plane at the same velocity and the 45 deg slope of the path means that the intersection between vortex and plane moves from pressure side to suction side at the rotor circumferential velocity u. In other words, we can safely assume the wake and vortex still have their original velocity and direction as they pass through L2F plane 1; they feel no

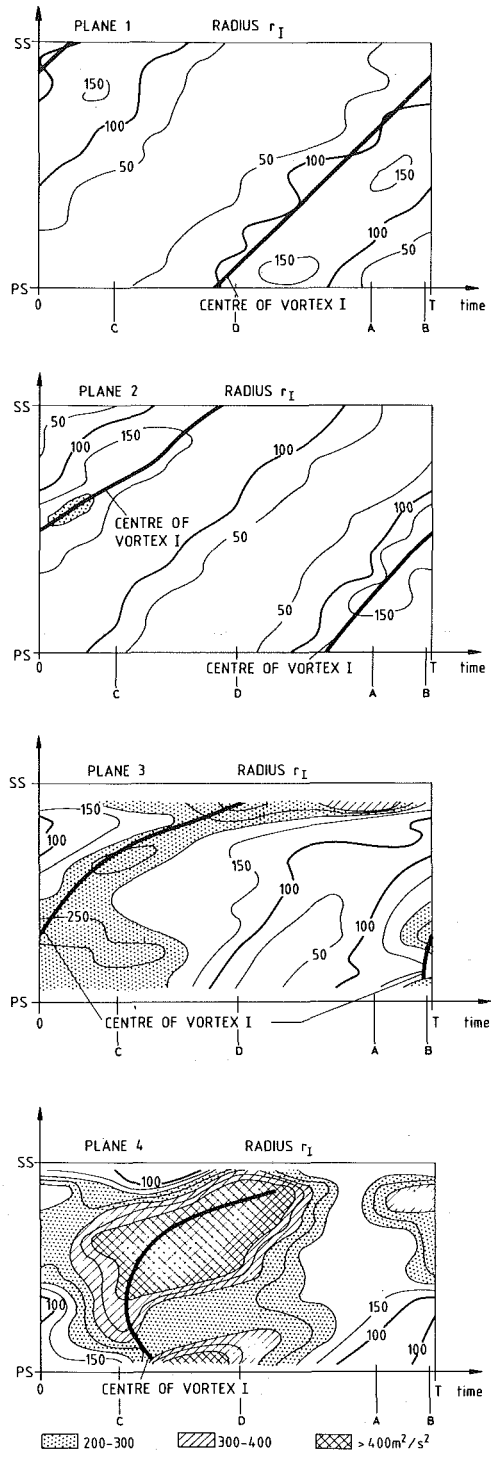

Fig. 7 Time-distance diagrams for vortex I contours of random unsteadiness $\tilde{c}_L'^2$

influence from the rotor yet. The streamwise component of the fluctuating kinetic energy $\tilde{c}_L'^2$ is seen to be in the range of 100 to 150 m^2/s^2.

As the vortex and wake pass through L2F plane 2, approximately 6 percent of axial chord forward of the nose, they begin to feel the influence of the blade. A small spot of higher turbulence appears near midchannel and the contour $\tilde{c}_L'^2 = 150$ m^2/s^2 extends more than halfway across the channel. The slope of the vortex path, i.e., its velocity along line *PS–SS*, decreases between midchannel and the suction side, indicating that the wake and vortex are decelerating in that half of the channel; that is, they arrive at the plane later than they would

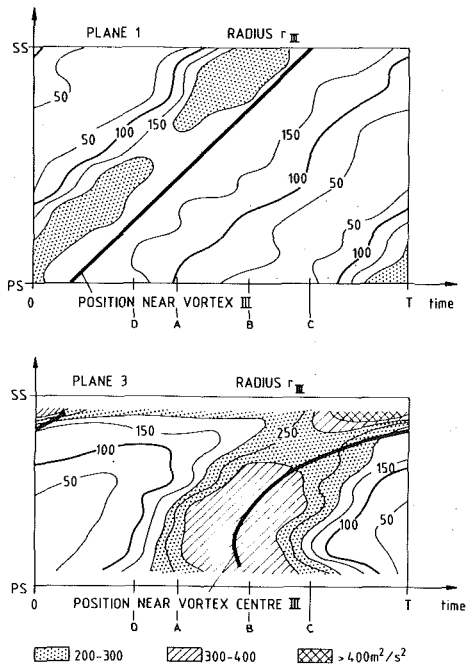

Fig. 8 Time-distance diagrams for vortex III contours of random unsteadiness $\tilde{c}_L'^2$

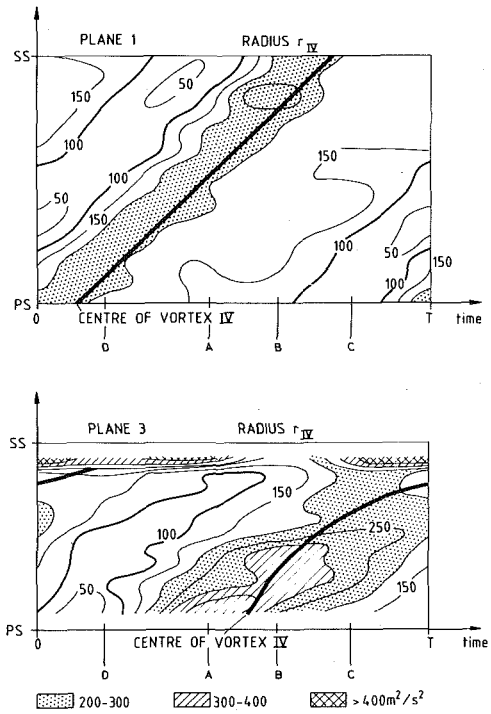

Fig. 9 Time-distance diagrams for vortex II contours of random unsteadiness $\tilde{c}_L'^2$

have with their original velocity. In physical space, the vortex and wake are aligning themselves more nearly in the axial direction as the suction-side velocity decreases and the mid-channel velocity continues. Fluid particles near the suction side cross the plane "behind schedule." In the pressure side the channel, the slope of the vortex path increases, indicating that the vortex and wake are aligning themselves toward the tangential direction. In physical space, the portions of the vortex and wake nearest the pressure side are caught in the stagnation region and therefore decelerate, while those near midchannel proceed with more or less their original velocity.

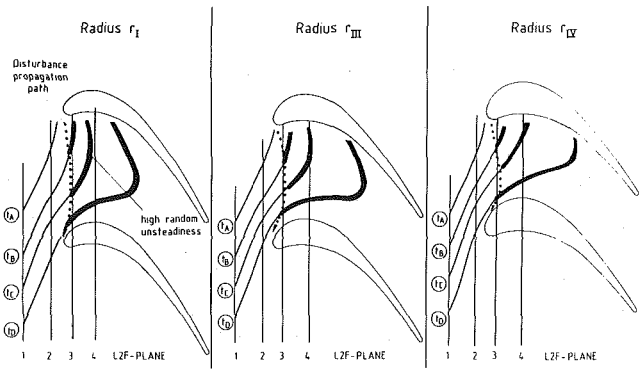

Fig. 10 Schematic of propagation of high turbulence zones

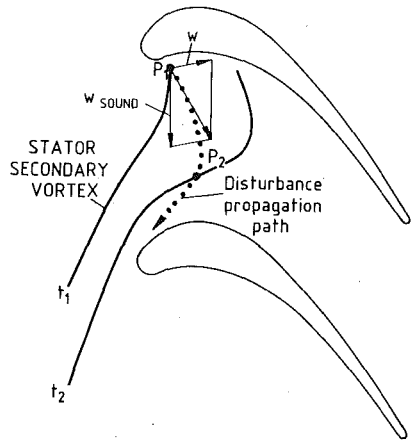

Fig. 11 Schematic of disturbance propagation

Again, the fluid particles near the blade cross the plane behind schedule.

In plane 3, approximately 6 percent of axial chord behind the nose, much the same situation exists, with one important difference. The vortex and wake have been cut off the pressure-side blade and a large zone of turbulence, in which $\tilde{c}_L'^2$ is in the range 200 to 250 m^2/s^2, extends completely across the channel, surrounding the vortex.

In the fourth L2F plane, some 25 percent of axial chord downstream of the nose, near the crown of the blade, the situation becomes chaotic. Very high turbulence, with $\tilde{c}_L'^2 \geq 400$ m^2/s^2 over a large region, fills the channel from side to side and persists for almost the entire vane passing period, although a slender zone of undisturbed fluid can still be seen. The slope of the vortex path is negative near the pressure side, indicating that the vortex is moving toward the blade, rather than away from it as before. In physical space, the vortex and wake have been pulled into the form of a bow whose open end points upstream (see Fig. 4). Therefore, they cross the plane in two places and the points of intersection move toward the two blades.

Figure 8 shows the time-distance diagrams for L2F planes 1 and 3 at radius r_{III}, near midspan. The heavy line marks a path just below that of vortex III, which turned out to lie slightly above the radius at which data were taken. The discussion of Fig. 7 applies here also, with a couple of additional comments. First, the vortex lies toward the pressure side of the incoming wake, whereas vortex I lay toward the suction side. Then, we see two tongues of high turbulence extending from the blade surfaces and following the vortex through plane 1. The incoming turbulence level is higher here than at radius r_I, exceeding 200 m^2/s^2 in the tongues. In plane 3, the situation for vortex III is almost identical to that for vortex I, with the exceptions that the suction side here is continuously bathed in turbulent fluid and the increase in turbulence over the incoming level is

smaller, reaching only 300 m^2/s^2, and is restricted to the pressure-side half of the channel.

The time–distance diagrams for vortex IV, which lies at approximately 1/4 span, are shown in Fig. 9. Note that on crossing L2F plane 1, the vortex is already surrounded by high turbulence, which, considering its location near the hub endwall, is not surprising. The situation in L2F plane 3 is similar to that at the other two radii except that the zone of high turbulence surrounding the vortex is narrower, i.e., it does not last as long, and the free-stream fluid penetrates briefly to the suction side. Note also that the increase of turbulence over the incoming level is again small, reaching only 350 m^2/s^2, and is confined to the pressure-side half and a small part of the suction side of the channel. Finally, note that all parts of the wake and vortex are moving toward the suction side of the channel as they cross plane 3 (the slope of the vortex is positive everywhere), even though they have been pulled into a bow in physical space.

It is clear from Figs. 7–9 that, in the rotor entrance region, the turbulence increases above the levels in the incoming wake, but only in areas associated with the stator secondary vortices. Outside the vortex areas, there was no discernible increase. The most reasonable explanation of this phenomenon is that the vortices break down and some of their kinetic energy is converted into turbulence [7, 13].

The vortex paths shown in the time–distance diagrams of Figs. 7–9 are shown in the blade-to-blade plane in Fig. 10. In Fig. 10(*a*), the locations of vortex I corresponding to the four instants in time *A*, *B*, *C*, and *D* from Fig. 7 are shown. At time t_A the vortex has not yet penetrated plane 3 and the turbulence level along it is essentially that of planes 1 and 2. At times t_B, t_C, and t_D, the vortex is passing through plane 3 and, as seen from the last two diagrams in Fig. 7, all of the vortex downstream of plane 3 is surrounded by high turbulence, indicated by heavy lines in Fig. 10. The upstream end of the high-turbulence area is found by axial interpolation to lie just forward of plane 3. At radii r_{III} and r_{IV} the behavior is similar except that at time t_C the high-turbulence zone does not quite extend forward to plane 3.

It is clear from study of Figs. 10 and 7 that the elevated turbulence spreads from the pressure side back along the vortex axis to approximately plane 3, but no further. Two questions are raised. Where exactly does the turbulence increase begin and why does it stop spreading where it does?

The model sketched in Fig. 11 explains: Slightly after the vortex is cut by the blade, for instance at point P_1, a disturbance is created which propagates along the vortex axis with the speed of sound. Simultaneously, the vortex is swept downstream at the local relative velocity. The resultant path is shown as a sequence of dots.

To get the best fit to the measurements, the origin of the turbulence increase (point P_1) is shifted slightly up- or downstream along the pressure side of the blade. The turbulence propagation paths which best match the measured results are marked by dots in Fig. 10. At each radius, excellent agreement with the measured results is apparent. The origin of turbulence production, as found by this model, occurs near the pressure-side stagnation region of the blades, immediately after the cutting of the stator secondary vortices.

Conclusions

L2F measurements in the rotor region of a single-stage, cold-air turbine have been analyzed with special regard to the unsteady blade row interaction caused by secondary vortices.

The behavior of the stator secondary vortices has been investigated as they propagate through the rotor. The following properties have been shown:

- The stator secondary vortices, which originally are aligned parallel to the stator wakes, are cut off by the rotor blades.
- Immediately after the vortex is cut off, the turbulence in the vortex region increases considerably. Most probably, the vortical motion breaks up and its energy is converted into turbulence.
- The origin of the breakdown is located near the pressure-side stagnation region of the rotor blades.
- The increase of turbulence spreads back along the vortex axis at the speed of sound.

References

1 Ashworth, D. A., La Graff, J. E., Schultz, D. L., and Grindrod, K. J., "Unsteady Aerodynamic and Heat Transfer Processes in a Transonic Turbine Stage," ASME JOURNAL OF ENGINEERING FOR GAS TURBINES AND POWER, Vol. 107, 1985, pp. 1022–1030.

2 Binder, A., "Turbulence Production Due to Secondary Vortex Cutting in a Turbine Rotor," ASME JOURNAL OF ENGINEERING FOR GAS TURBINES AND POWER, Vol. 107, 1985, pp. 1039–1046.

3 Binder, A., "Instationäre Strömungsvorgänge im Laufrad einer Turbine," submitted 1985.

4 Binder, A., and Romey, R., "Secondary Flow Effects and Mixing of the Wake Behind a Turbine Stator," ASME JOURNAL OF ENGINEERING FOR POWER, Vol. 105, 1983, pp. 40–46.

5 Binder, A., Förster, W., Kruse, H., and Rogge, H., "An Experimental Investigation Into the Effects of Wakes on the Unsteady Turbine Rotor Flow," ASME JOURNAL OF ENGINEERING FOR GAS TURBINES AND POWER, Vol. 107, 1985, pp. 458–466.

6 Förster, W., and Mach, K., "Instationäre Strömung in einem Turbinenlaufrad," VDI-Berichte 572, 1985.

7 Hall, M. G., "The Structure of Concentrated Vortex Cores," *Progress in Aeron. Science*, Vol. 107, 1966, pp. 53–110.

8 Hawthorne, W. R., "Rotational Flow Through Cascades, Pt. I: The Components of Vorticity," *Q. J. Mech. and Appl. Math.*, Vol. VIII, Pt. 3, 1955.

9 Hodson, H. P., "An Inviscid Blade-to-Blade Prediction of a Wake-Generated Unsteady Flow," ASME JOURNAL OF ENGINEERING FOR GAS TURBINES AND POWER, Vol. 107, 1985, pp. 337–344.

10 Hodson, H. P., "Measurements of Wake Generated Unsteadiness in the Rotor Passages of Axial Flow Turbines," ASME JOURNAL OF ENGINEERING FOR GAS TURBINES AND POWER, Vol. 107, 1985, pp. 467–476.

11 Horlock, J. H., "Recent Developments in Secondary Flow," AGARD-CP-214, 1977.

12 Joslyn, H. D., Caspar, J. R., and Dring, R. P., "Inviscid Modeling of Turbomachinery Wake Transport," 21st Joint Propulsion Conference, 1985, Paper No. AIAA-85-1132.

13 Leuchter, O., and Solignac, J. L., "Experimental Investigation of the Turbulent Structure of Vortex Wakes," ONERA-Report T. P. 1983–107.

14 Schodl, R., "Entwicklung des Laser-Zwei-Fokus-Verfahrens für die berührungslose Messung von Strömungsvektoren, insbesondere in Turbomaschinen," Dissertation TH Aachen, 1977.

15 Schodl, R., "A Laser-Two-Focus (L2F) Velocimeter for Automatic Flow Vector Measurements in the Rotating Components of Turbomachines," ASME *Journal Fluids Engineering*, Vol. 102, 1980, pp. 412–419.